Hydrometallurgy 246 (2026) 106884

Contents lists available at ScienceDirect

Hydrometallurgy

journal homepage: www.elsevier.com/locate/hydromet

Tailoring the microstructure of microporous organic-inorganic hybrid SiO_2 membranes for separation of P204 (D2EHPA) and Na_2SO_4 in spent battery process wastewater: Successes and challenges

Yuanyan Liu, Xinyu Jiao, Xincheng Pan, Hong Qi *

College of Chemical Engineering, Nanjing Tech University, Nanjing 210009, China

ARTICLE INFO

Keywords:
1,2-bis(triethoxysilyl) ethane
Polyethyleneimine
Membrane
di-(2-ethylhexyl) phosphoric acid

ABSTRACT

To address the wastewater treatment challenge involving di-(2-ethylhexyl) phosphoric acid (P204), this study employed membrane separation techniques to investigate the separation of the P204/Na_2SO_4 system. Using 1,2-bis(triethoxysilyl) ethane (BTESE) as the precursor, an organic-inorganic hybrid SiO_2 membrane was prepared with the sol-gel method. The resultant pure BTESE membrane exhibited a pure water permeation coefficient of 42.3 L m^{-2} h^{-1} bar^{-1}. The rejection for P204 and Na_2SO_4 were 91.0% and 87.7%, respectively, indicating an inability to achieve effective separation of the two substances. To reduce the rejection of Na_2SO_4, a BTESE/PEI composite membrane was constructed by coating polyethyleneimine (PEI) on the surface of the BTESE membrane. The introduced PEI endowed the membrane with positive surface charges, achieving a synergistic separation effect combining size sieving and electrostatic repulsion. The results showed that the pure water permeation coefficient of the BTESE/PEI-0.1 wt% (BP-0.1 wt%) composite membrane was 36.4 L m^{-2} h^{-1} bar^{-1}, with the rejection for P204 remaining at 85.9%, while the rejection for Na_2SO_4 decreased to 19.0%, successfully achieving the selective separation of the two substances. Nevertheless, when applied to real high-salt wastewater, the rejection of P204 and Na_2SO_4 drop sharply to 20.7% and 14.6%, respectively. Such performance degradation is mainly attributed to the salting-out effect under high-salt conditions. It distorts the solvation layer and aggregation state of P204 molecules, allowing P204 to pass through membrane pores and deteriorating the membrane's selective separation ability.

1. Introduction

The rapid expansion of the new energy vehicle industry has driven a continuous surge in the volume of retired power batteries (Lee et al., 2025). Improper disposal or random discard of spent batteries tends to result in resource wastage and heavy metal contamination (Luo et al., 2015). Currently, the solvent extraction method is the most widely used process in the recycling of waste batteries (Lim et al., 2025). Commonly used extractants include di-(2-ethylhexyl) phosphoric acid (P204, also known as D2EHPA), 2-ethylhexyl phosphonic acid mono-2-ethylhexyl ester (P507), and bis(2,4,4-trimethylpentyl) phosphonic acid (Cyanex 272) (Yang et al., 2016). P204 is an acidic extractant (see Fig. 1) with a molecular structure centered on the phosphate group and combined with organic long-chain alkanes. It exhibits excellent metal complexation ability and organic phase solubility, and is widely used in industrial fields such as nuclear fuel extraction, rare earth element separation and non-ferrous metal extraction (Jiang et al., 2025; Liu et al., 2019).

However, the rapid expansion of the new energy industry has led to significant challenges concerning the management and compliance discharge of P204-containing wastewater. As illustrated in Fig. 2, multiple wastewater streams are generated throughout the hydrometallurgical recycling process. Among these, wastewater generated from the extraction section, which is characterized by high salinity and residual extractant, represents a typical refractory effluent. Conventional treatment generally involves organic removal and evaporation crystallization, whereas the present study explores membrane separation as an alternative approach for the selective separation of P204 and Na_2SO_4 from this wastewater.

Regarding the treatment of wastewater containing phosphorus-based extractants, several studies have been conducted. Su et al. (2018) and Liu et al. (2022) employed D201-OH strong basic anion exchange resin

* Corresponding author.
E-mail address: hqi@njtech.edu.cn (H. Qi).

https://doi.org/10.1016/j.hydromet.2026.106884
Received 23 April 2026; Received in revised form 28 August 2026; Accepted 29 August 2026
Available online 30 August 2026
0304-386X/© 2026 Published by Elsevier B.V.

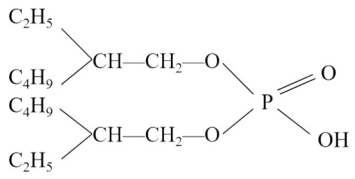


Fig. 1. Molecular structure of P204 (D2EHPA).

and DA201-C macroporous adsorption resin, respectively, to treat P507-containing wastewater. The results showed that both resins could achieve adsorption equilibrium within 20 min, with removal efficiencies exceeding 95%, demonstrating high-performance treatment characteristics. However, strong chemical interactions between the resins and organic phosphorus compounds hinder effective regeneration, resulting in substantial generation of recalcitrant solid waste (Su et al., 2018). This drawback severely limits the industrial application of the adsorption resin process. Oxidation technologies have also been applied for the treatment of phosphorus-containing extractant wastewater. Wang et al. (2023) used catalytic ozonation to treat P507-containing wastewater, achieving significant degradation of organic pollutants. In other studies, three-dimensional electrocatalytic oxidation technology (Wang et al., 2024) was employed to treat P204-containing wastewater, achieving a chemical oxygen demand (COD) removal efficiency of 93.5% under optimal operating conditions, with the system exhibiting desirable stability and catalytic activity.

Membrane separation technology has the advantages of low energy consumption, high efficiency, simple operation, continuous operation capability, and easy coupling with other processes. It is suitable for the treatment of wastewater containing extractants and can replace the evaporation crystallization and organic removal steps shown in Fig. 2. However, wastewater containing extractants such as P204 often has a complex composition, typically containing high concentrations of inorganic salts, substantial amounts of organic by-products, and emulsified droplets, which impose high requirements on the solvent resistance of membrane materials. Compared with polymer membranes, ceramic membranes, a type of inorganic membrane, exhibit advantages such as narrow and uniform pore size distribution, excellent chemical stability, and strong hydrophilicity (Chen et al., 2020; He et al., 2019; Luan et al., 2022). Moreover, the extractants and inorganic salts in the wastewater system both have relatively small molecular sizes (within approximately 2 nm). In this context, the advantages of organic-inorganic hybrid SiO_2 membranes become even more prominent. The 1,2-bis(triethoxysilyl) ethane (BTESE) based organic-inorganic hybrid SiO_2 membrane combines the performance advantages of both organic and inorganic membranes, offering not only high selectivity and chemical stability but also a simple preparation process and recyclability. Current authors' research group has also conducted in-depth studies on BTESE membranes in recent years. The BTESE membrane prepared by tuning the sol formulation exhibits a pore size distribution primarily centered around 0.7 nm (Zhang et al., 2021). From the perspective of the size exclusion mechanism, this nanofiltration membrane is expected to possess ideal separation performance capable of meeting the requirements for treating such wastewater. Therefore, this study aims to investigate the separation of a P204/Na_2SO_4 system using membrane separation technology, with the goal of providing a theoretical basis and reference for the practical industrial application of this technology.

However, it is worth noting that Wu et al. (2020) applied a BTESE membrane prepared on an Al_2O_3 ceramic support to the separation of magnesium and lithium, achieving over 90% rejection of Na_2SO_4. This is attributed to the strong electrostatic repulsion between the negatively charged membrane and SO_4^{2-} ions in the solution. To maintain electrical neutrality in the solution, Na^+ ions coexist with SO_4^{2-}, resulting in the rejection of Na_2SO_4 on the membrane side and thus high rejection of Na_2SO_4 (Nicolini et al., 2016; Suhalim et al., 2022; Wai Lin et al., 2007). Consequently, even if P204 is effectively retained, Na_2SO_4 can hardly permeate through the membrane, which is unfavorable for the selective separation of the two components. To mitigate excessive Na_2SO_4 rejection, a rational strategy is surface charge modulation. Polyethyleneimine (PEI), owing to its high density of primary and secondary amine group, is widely employed to impart positive surface charge to nanofiltration membranes. Lin et al. (2019) developed PMIA/PEI composite nanofiltration membranes using poly(*m*-phenylene isophthalamide) (PMIA) and PEI, achieving Na_2SO_4 rejection below 20%. Similarly, Gu et al. (2019) fabricated positively charged composite nanofiltration membranes via interfacial cross-linking of PEI with trimeric acid (TMA) and reported a markedly reduced Na_2SO_4 rejection of only 8.8%. Based on these findings, effective separation of P204 from Na_2SO_4 necessitates a dual-mechanism design. The large P204 molecule (with a hydrodynamic diameter of approximately 1.1 nm (Bapat and Dalvi, 2019)) is retained by a size-exclusion process, and the electrostatic facilitation of Na_2SO_4 permeation is achieved through a positively charged membrane surface. This process, therefore, enables synergistic and charge-enhanced selectivity.

In this work, BTESE hybrid membranes were fabricated on tubular Al_2O_3 supports via the sol-gel method. Filtration tests using P204/Na_2SO_4 mixed feed revealed high rejection of P204 (91.0%) and Na_2SO_4 (87.7%), meaning both solutes were largely retained simultaneously. To reduce the rejection of Na_2SO_4 and achieve selective separation of the two components, PEI was further coated onto the BTESE membrane surface. The resultant composite membrane inherits the small pore-size feature of pristine BTESE membrane while introducing positively charged groups from PEI, thus establishing a synergistic separation mechanism combining size sieving and electrostatic repulsion. Experimental results demonstrate that the optimized BP-0.1 wt% composite membrane maintains a high P204 rejection of 85.9% and sharply reduces Na_2SO_4 rejection to 19.0%, achieving efficient selective separation of the P204/Na_2SO_4 system. Accordingly, membrane separation shows promising application potential for this separation system and deserves further development toward practical industrial scaling.

2. Experimental

2.1. Preparation of BTESE sol

The BTESE sol was prepared via a sol-gel process, as described below. First, 5 mL of BTESE and 10 mL of anhydrous ethanol were added to a vessel, which was then immediately placed in an ice bath and stirred continuously to ensure thorough mixing. Subsequently, a mixture consisting of 5 mL of anhydrous ethanol, 5 mL of deionized water, and 0.5 mL of 1 mol L^{-1} HCl was added dropwise to the BTESE/EtOH solution using a constant-pressure dropping funnel. During the dropwise addition, magnetic stirring was maintained to ensure sufficient reaction and prevent aggregation or precipitation induced by local high concentrations of the reactants. After the completion of addition, the resulting mixture was heated to 60 °C in a thermostatic water bath and allowed to react under reflux for 1.5 h. At the completion of the reaction, the mixture was allowed to cool spontaneously to room temperature. Finally, it was filtered through a 0.22 μm syringe filter, thus producing a homogeneous BTESE solution.

2.2. Preparation of pristine BTESE and BTESE-based membranes

A BTESE coating solution was prepared by diluting an appropriate volume of BTESE sol with anhydrous ethanol to achieve a silicon concentration of 0.17 mol L^{-1}. The inner surface of the tubular Al_2O_3 support was uniformly coated with this solution via dip-coating: the immersion duration was fixed at 5 s, and the withdrawal speed was controlled at 0.5 cm s^{-1}. Subsequently, the coated membrane was dried in a climate-controlled chamber at 40 °C and 25% relative humidity for 1 h. Following drying, the membrane was subjected to thermal treatment in a nitrogen-purged tube furnace under the following conditions:

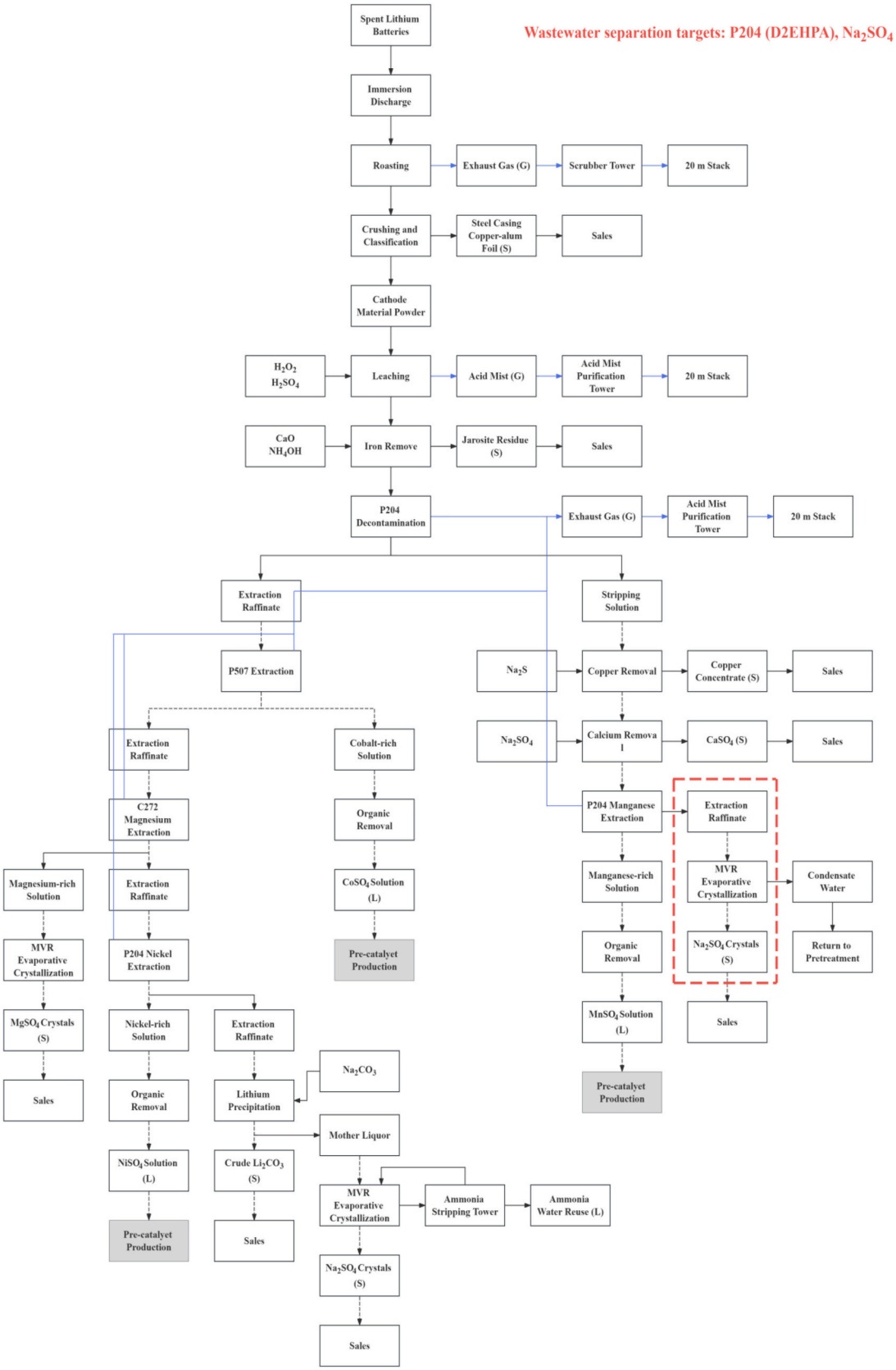


Fig. 2. Processing flowchart for handling used lithium-ion batteries (Zhan et al., 2020).

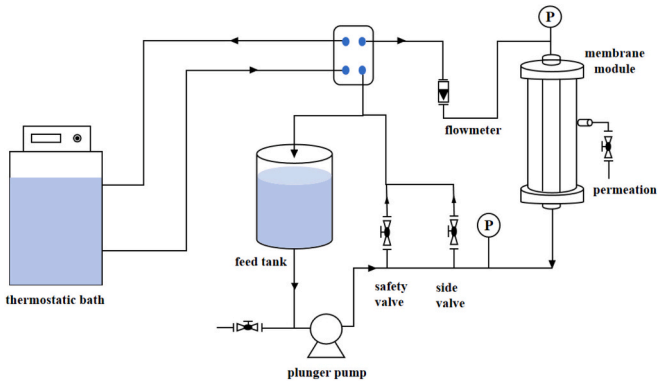


Fig. 3. Schematic diagram of tubular membrane cross-flow filtration device.

N_2 flow rate of 50 mL min^{-1}, a heating/cooling rate of 0.5 °C min^{-1}, a calcination temperature of 400 °C, and a dwell time of 3 h. To minimize defect formation and enhance membrane integrity, a secondary dip-coating step was performed on the calcined BTESE hybrid membrane. In this step, the immersion time was reduced to 1 s, while all other parameters remained identical to those of the first coating cycle, including solvent composition, withdrawal speed, drying conditions, and thermal treatment parameters.

Separately, PEI solutions of varying mass fractions (0.03, 0.05, 0.07, and 0.1 wt%) were prepared by dissolving predetermined masses of PEI polymer in deionized water, followed by magnetic stirring at ambient temperature until complete dissolution was achieved. The resulting PEI solutions were used to impregnate the BTESE hybrid membrane via immersion for 2 h. After impregnation, the membranes were dried in an electrically heated and forced-air convection oven at 40 °C for 12 h. The final products were designated as BP-x wt% (x = 0.03, 0.05, 0.07, 0.1), representing the nominal PEI loading in the BTESE-PEI tubular hybrid membranes.

2.3. Evaluation of membrane performance

A custom-designed tubular ceramic membrane cross-flow filtration system was employed to evaluate the pure water flux, Na_2SO_4 single-solute rejection, and rejection behavior of a multi-component P204/Na_2SO_4 mixed solution using the BP membrane. The experimental setup is illustrated in Fig. 3. Pure water flux measurements were conducted at transmembrane pressures of 2, 3, 4, 5, and 6 bar (1 bar = 101.3 kPa). Aqueous feed solutions were prepared in two groups for comparative rejection assessment: (i) 1 mM Na_2SO_4 solution; and (ii) a mixture of P204/Na_2SO_4 with a mass ratio of 1:1. Rejection experiments were performed at a constant pressure of 5 bar, following a 40-min stabilization period to ensure steady-state filtration conditions. All the data were obtained by averaging the results of four repeated measurements. The Na_2SO_4 rejection was quantified via electrical conductivity measurements (using a calibrated conductivity meter) of both feed and permeate streams, while P204 rejection was determined by total organic carbon (TOC) analysis using a Shimadzu TOC-L CPH analyzer. Pure water permeability, J (L m^{-2} h^{-1} bar^{-1}), and solute rejection, R (%), were calculated with Eqs. (1) and (2):

$$J = \frac{V}{A \bullet t \bullet \triangle P} \tag{1}$$

$$R = \left(1 - \frac{C_p}{C_f}\right) \times 100\% \tag{2}$$

where V (L) denotes the permeate volume collected over time t (h); A (m^2) is the effective membrane area; ΔP (bar) is the applied transmembrane pressure; and C_f and C_p represent the solute concentrations (in equivalent units) in the feed and permeate streams, respectively.

3. Results and discussion

3.1. Characterization of BTESE-based membrane materials

Zeta potential and water contact angle (WCA) measurements were performed to systematically characterize the surface charge properties and interfacial wettability of the BP-x wt% composite nanofiltration membranes prepared with varying PEI doping concentrations. As illustrated in Fig. 4a, the induction of positive membrane surface charge following PEI incorporation resulted in a complete reversal of the initial negative charge. This transition is mainly attributed to the cross-linking interaction between PEI and the BTESE matrix, as well as the protonatable primary and secondary amine groups (-NH_2/-NH-) in the branched structure of PEI. These factors contribute to the formation of a strong cationic surface charge under aqueous conditions (Xiang et al., 2025). In the absence of PEI, the pristine BTESE membrane showed a zeta potential of −8.34 mV. Following the addition of PEI, a rapid shift in surface potential toward positive values was observed. At a PEI

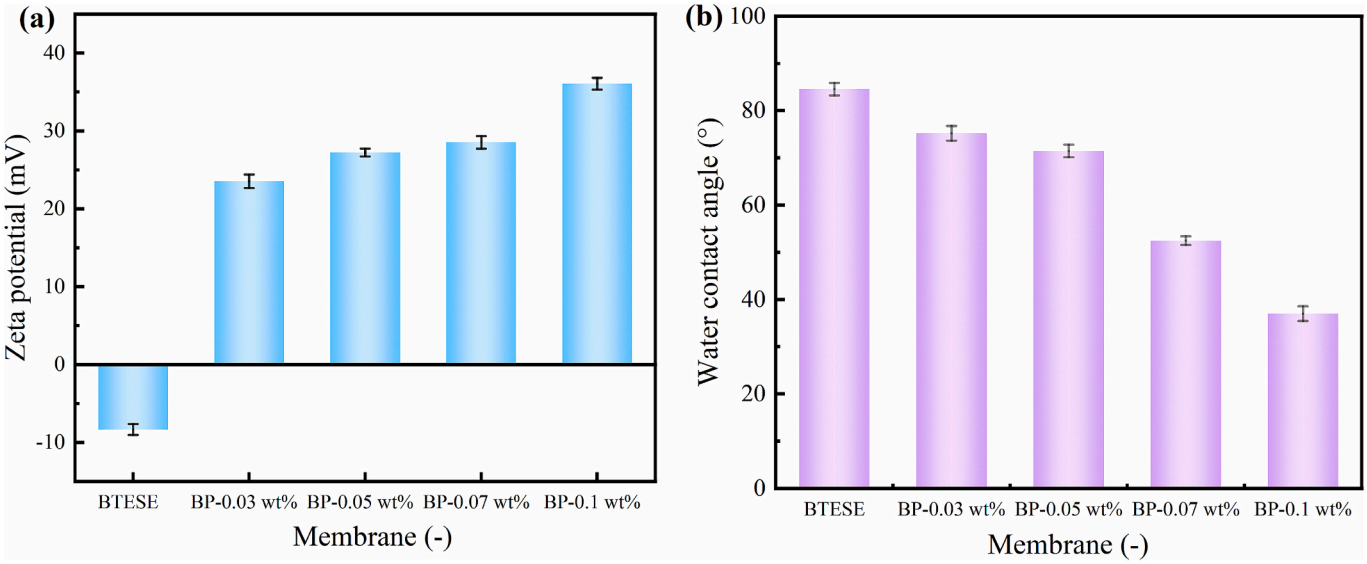


Fig. 4. (a) Surface zeta potential and (b) water contact angle of the BTESE-based membranes (temperature = 25 °C; pH = 6).

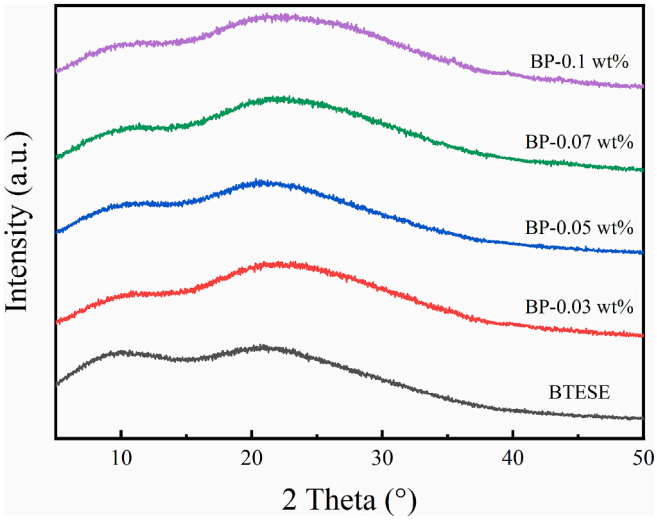


Fig. 5. XRD patterns of the BTESE-based membranes.

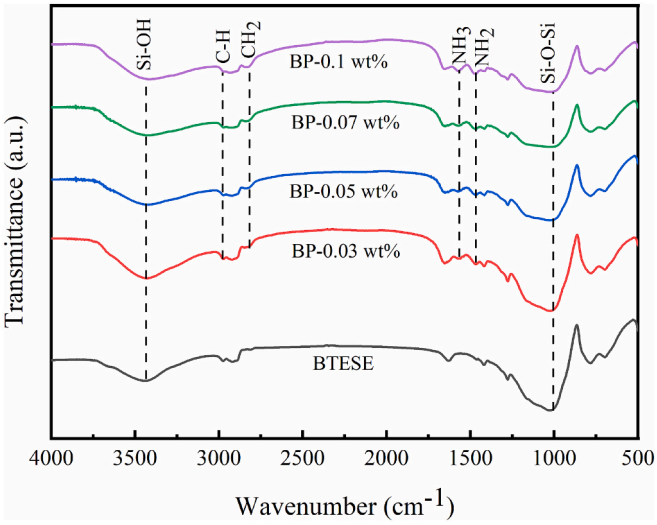


Fig. 6. FTIR patterns of the BTESE-based membranes.

doping concentration of 0.1 wt%, the BP-0.1 wt% membrane attained a zeta potential of +36.07 mV. Consistent with this trend, WCA measurements (Fig. 4b) indicated that the initial WCA of the neat BTESE membrane was 84°, while the incorporation of 0.1 wt% PEI reduced the WCA to 37°, suggesting significantly enhanced surface hydrophilicity. This improvement can be ascribed to the introduction of highly hydrophilic amine functionalities, which effectively regulate the interfacial energy and counteract the hydrophobic tendency resulting from the condensation and consumption of silanol (Si-OH) groups during the high-temperature calcination of BTESE (Xu et al., 2020; Zhang et al., 2025). Furthermore, the gradual increase of the PEI loading increased the surface density of hydrophilic functional groups, allowing precise and tunable control over the membrane surface wettability.

The crystal structure of the BTESE-based membranes were characterized by X-ray diffraction (XRD), with the results presented in Fig. 5. As Fig. 5 shows, both the pristine BTESE membrane and the BP composite membranes modified with different concentrations of PEI display significantly broadened and diffused diffraction peaks in the 2θ range of 5–40°. No sharp characteristic diffraction peaks corresponding to crystalline phases were detected. These observations are consistent with previous reports (Li et al., 2021; Oh et al., 2020). Broadened diffraction peaks represent the typical structural signature of amorphous materials,

Table 1
FTIR characteristic peaks of BTESE and BP membranes.

Probable assignments	Wave number, cm^{-1}		Ref.
	BTESE	BP	
Si-OH	3650–3200		(Al-Oweini and El-Rassy, 2009; Ngamou et al., 2013)
Si-O-Si	1100-1000		
C-H	/	3000–2800	(Li et al., 2024; Nakahiro et al., 2021)
N-H	/	1650-1550	

indicating that the as-prepared BTESE-based hybrid membrane possesses a predominantly amorphous structure characterized by short-range ordering and long-range disorder. These five materials exhibit pronounced amorphous characteristics and structural disorder, further verifying that no distinct crystalline domains are formed in such organic-inorganic hybrid membranes during calcination and interfacial cross-linking.

This study further characterized the chemical composition of the BTESE-based membranes using fourier-transform infrared spectroscopy (FTIR) and X-ray photoelectron spectroscopy (XPS). As illustrated in Fig. 6, the FTIR spectrum of the pristine BTESE membrane presents a broad and strong absorption band centered at 3650–3200 cm^{-1}, which can be assigned to the stretching vibration of incompletely condensed silanol (Si-OH) groups (Al-Oweini and El-Rassy, 2009; Ngamou et al., 2013), and relevant data are listed in Table 1. This result confirms that the residual Si-OH functionalities remain after the hydrolysis and condensation of the BTESE precursor. The introduction of PEI resulted in a progressive reduction of the intensity of the Si-OH band across all BP composite membranes. This finding suggests the occurrence of interfacial interactions between the primary amino groups ($-NH_2$) of PEI and the silanol groups of BTESE. These interactions, likely to involve hydrogen bonding and/or condensation reactions, effectively reduce the content of free Si-OH groups and enhance the interfacial compatibility between the organic and inorganic phases. Notably, no obvious absorption peaks appear at 3000–2800 cm^{-1} (C—H stretching of PEI alkyl chains) or 1650–1550 cm^{-1} (N—H bending vibration of PEI amine groups) in the pure BTESE membrane (Li et al., 2024; Nakahiro et al., 2021). In contrast, all BP composites show distinct peaks in these two regions, whose intensities are dependent on the PEI concentration. The gradual enhancement of these bands with increasing PEI loading provides direct spectroscopic evidence for the successful incorporation of PEI into the BTESE matrix. Furthermore, the presence of a robust absorption band within the range of 1100–1000 cm^{-1}, ascribed to the asymmetric stretching vibration of the Si-O-Si network, is clearly observed in all samples (Al-Oweini and El-Rassy, 2009; Ngamou et al., 2013). This observation verifies the formation of a stable and cross-linking silica framework in the composite membranes.

Meanwhile, related data for XPS spectral are shown in Fig. 7 and Table 2. Full-spectrum XPS analysis (Fig. 7a) reveals that the pristine BTESE membrane exhibits only characteristic peaks of O 1s (~532 eV), C 1s (~285 eV), and Si 2p (~102 eV), with no detectable nitrogen signal, which is fully consistent with its stoichiometric composition. Upon incorporation of PEI, distinct N 1s peaks (~400 eV) appear in all BP composite membranes, and their intensities increase gradually with the increase of PEI loading, providing direct evidence for the successful integration of PEI into the BTESE matrix. Notably, the binding energies of the O 1s, C 1s, and Si 2p peaks remain almost unchanged across all samples (Zheng et al., 2022), indicating that the inherent Si-O-Si network of BTESE is well preserved. This suggests that PEI modification occurs mainly at the interfacial region, rather than within the bulk silica framework. For the BP-0.1 wt% sample with the highest PEI content, high-resolution N 1s deconvolution (Fig. 7b) resolved three chemically distinct nitrogen species (Xing et al., 2023). Firstly, a peak at 398.6 eV was assigned to primary amine groups (-NH_2), corresponding to unbound, non-interacting amine sites. Secondly, a peak at 399.5 eV was attributed to secondary amine groups (-NH-), indicative of

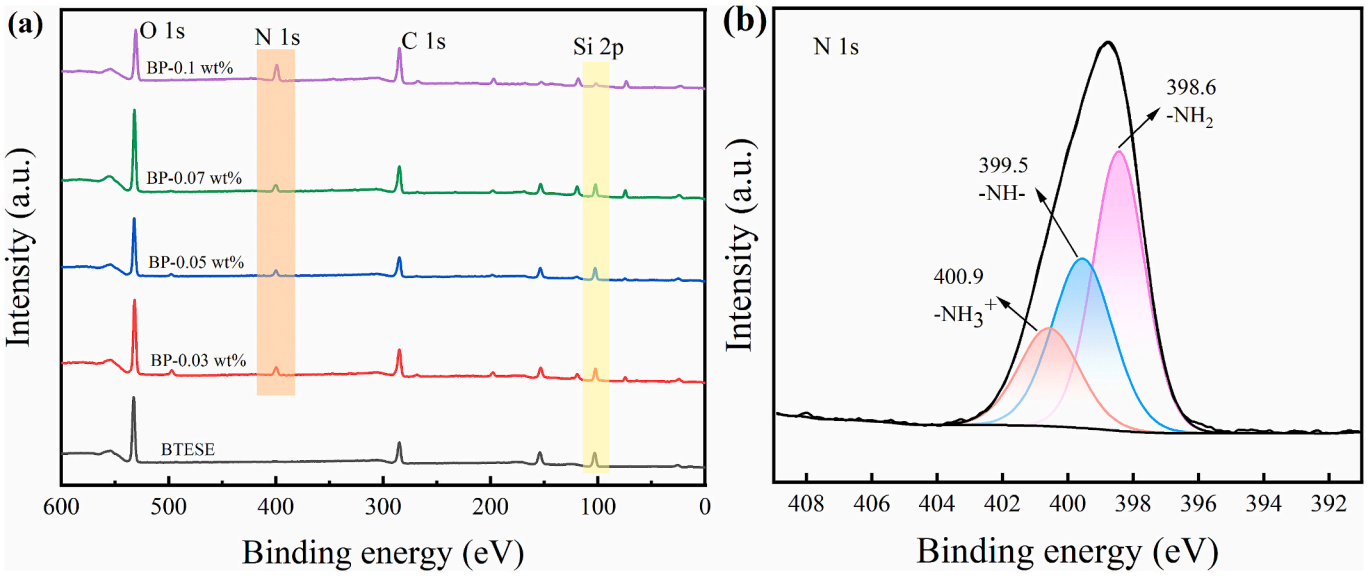


Fig. 7. (a) XPS full spectra of the BTESE-based membranes and (b) detailed N element spectrum of the BP-0.1 wt% membrane.

Table 2
XPS spectral data for BTESE and BP membranes.

Probable assignments	Binding energy, eV		Ref.
	BTESE	BP	
Si 2p	102	102	(Xing et al., 2023; Zheng et al., 2022)
N 1s (-NH_2)	/	398.6	
N 1s (-NH-)	/	399.5	
N 1s (-NH_3^+)	/	400.9	

hydrogen bonding or condensation reactions between PEI amines and surface silanol (Si-OH) groups of BTESE. Thirdly, a peak at 400.9 eV corresponded to protonated amine species (-NH_3^+), likely formed by partial protonation under the mildly acidic environment generated during BTESE hydrolysis or at the polymer-silica interface. Collectively, the presence of N 1s spectral features indicates the occurrence of significant interfacial chemical interaction between PEI and BTESE. These interactions are not merely a physical blending process involving hydrogen bonding and covalent-like coupling. This interpretation is supported by quantitative analysis that demonstrates significantly enhanced interfacial compatibility and effective surface functionalization of the BTESE membrane by PEI.

The surface morphology and cross-sectional architecture of the BTESE-based composite nanofiltration membranes were systematically characterized utilizing the technique of scanning electron microscopy (SEM). As shown in Fig. 8, all five membranes display highly uniform, smooth, and defect-free surfaces, with no macroscopic cracks, pinholes, or discontinuities observed. Cross-sectional SEM analysis reveals well-defined, stratified structures across all samples. The pristine BTESE membrane has a thickness of 767 nm. Upon incorporation of PEI, the thickness of the BP composite membranes gradually increases to 840 nm, 883 nm, 899 nm, 909 nm, respectively, corresponding to the increasing PEI loading concentrations. This consistent, concentration-dependent thickness variation strongly indicates the successful integration of PEI into the BTESE matrix and its active involvement in the formation and structural evolution of the selective layer.

3.2. *Pure water permeation performance of BTESE-based membrane materials*

The pure water performance of five BTESE-based membranes was evaluated under transmembrane pressures ranging from 2 to 6 bar using a custom-built tubular cross-flow filtration system (Fig. 3). These membranes included the pristine BTESE membrane and four PEI-modified variants, which were denoted as BP-0.03 wt%, BP-0.05 wt%, BP-0.07 wt%, and BP-0.1 wt%. As illustrated in Fig. 9, the pure water flux of all membranes demonstrated a linear increase with increasing transmembrane pressure. This finding aligns with the principles outlined by Darcy's law. The pristine BTESE membrane achieved a pure

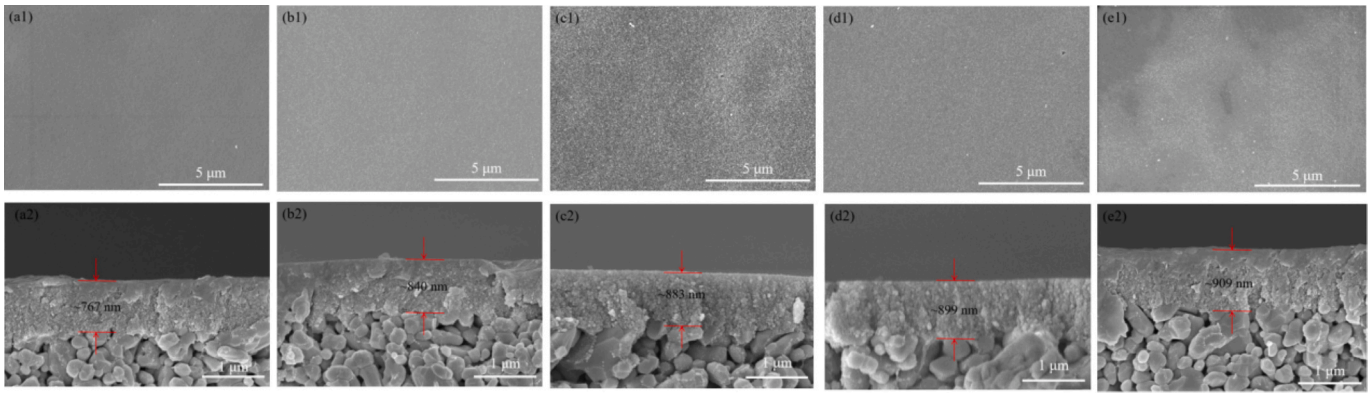


Fig. 8. SEM images of the surface (1) and cross-section (2) of the (a) BTESE, (b) BP-0.03 wt%, (c) BP-0.05 wt%, (d) BP-0.07 wt%, (e) BP-0.1 wt% membrane.

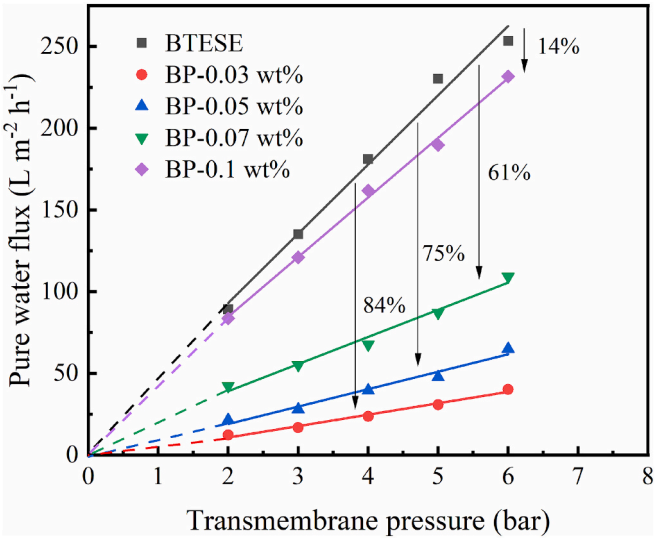


Fig. 9. Variation of pure water flux of the BTESE-based membranes with the transmembrane pressure difference Data are obtained from repeated measurements, the same for Figs. 10 and 11.

water permeability coefficient of 42.3 L m^{-2} h^{-1} bar^{-1}. In contrast, the PEI modification induced a pronounced reduction in permeability at low PEI loadings. Relative to the pristine membrane, the flux decreased by 84%, 75%, and 61% for BP-0.03 wt%, BP-0.05 wt%, and BP-0.07 wt%, respectively. This decline is attributed to the formation of a thin PEI coating on the membrane surface, which increases the effective thickness of the membrane and thereby extends the diffusion path for water molecules, elevating hydraulic resistance. However, at the highest PEI loading of 0.1 wt%, the flux recovered substantially to 36.4 L m^{-2} h^{-1} bar^{-1}, which represents only a 14% reduction versus the pristine membrane. This improvement is ascribed to enhanced surface hydrophilicity imparted by the higher PEI content, which mitigates interfacial resistance to water transport and partially offsets the adverse effect of increased thickness.

3.3. Separation performance of BTESE-based membrane materials for P204/Na_2SO_4

To systematically evaluate the separation performance of five BTESE-based membranes (namely the pristine BTESE membrane and four branched PEI-modified membranes) for Na_2SO_4 and P204, rejection experiments were conducted using (i) a 1 mM single-component Na_2SO_4 aqueous solution and (ii) a multi-component P204/Na_2SO_4 mixture with a mass ratio of 1:1. As illustrated in Fig. 10(a), the rejection of Na_2SO_4 for the five membranes in the single-component solution was 94.4%, 28.6%, 25.9%, 19.8%, and 14.0%, respectively. The pristine BTESE membrane exhibited markedly higher Na_2SO_4 rejection, while all PEI-modified membranes showed substantially reduced rejection, which is consistent with progressive attenuation as PEI loading increased. This trend is primarily attributable to charge modulation: PEI introduces abundant primary and secondary amine groups that neutralize the intrinsic negative surface charge of the BTESE matrix. Consequently, electrostatic repulsion against SO_4^{2-} anions is weakened, facilitating enhanced anion permeation and lowering overall Na_2SO_4 rejection. At a PEI loading of 0.1 wt%, the rejection dropped to 14.0%, which reflects intensified positive surface charge density and further diminished Donnan exclusion.

Fig. 10(b) presents the rejection performance in the mixture of P204/Na_2SO_4 with a mass ratio of 1:1. All five membranes achieved high P204 rejection, with values of 91.0%, 74.4%, 82.1%, 77.7%, and 85.9% respectively. This indicates that P204 separation is predominantly governed by size-exclusion mechanisms. This observation is consistent with the known tendency of P204 to form dimers in aqueous solutions. The large hydrodynamic diameter of P204 renders it effectively retained even by relatively tight membranes. In contrast, Na_2SO_4 rejection in the mixed solution closely mirrored that observed in the single-component tests: the pristine BTESE membrane maintained high rejection at 87.7%, while the PEI-modified membranes exhibited significantly lower rejection with values of 32.2%, 27.2%, 22.3%, and 19.0%, respectively. Collectively, the findings indicate that the pristine BTESE membrane shows inadequate selectivity for effective P204/Na_2SO_4 separation, attributable to its concurrent high rejection of both species. In contrast, PEI modification imparts differential transport behavior, characterized by high P204 rejection coupled with low Na_2SO_4 rejection. This, in turn, enables promising separation selectivity between the two solutes in the solution.

Based on the above analyses of the chemical composition, microstructure, and separation performance of the BP membranes, Fig. 11 presents a proposed schematic illustration of the membrane structure. The BTESE membrane possesses a Si-O-Si network structure with relatively small pores, which can effectively hinder the permeation of P204 with a large molecular size. However, the negatively charged membrane

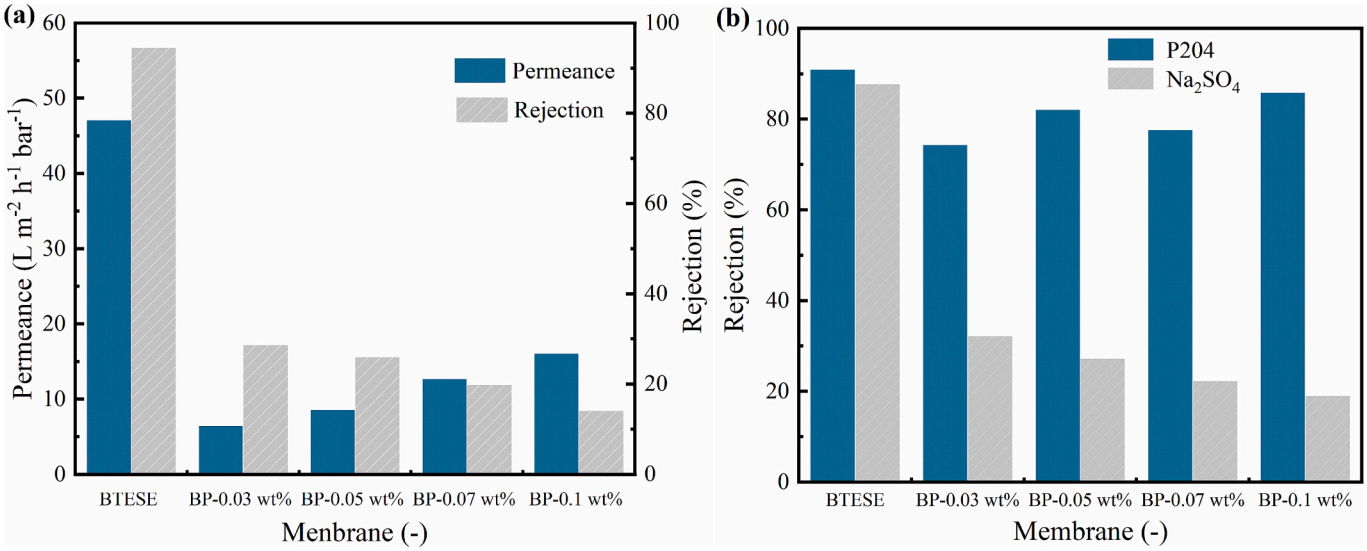


Fig. 10. Permeance and rejection by the BTESE-based membranes in (a) 1 mM Na_2SO_4 solution (b) P204/Na_2SO_4 mixed solution with a mass ratio of 1:1.

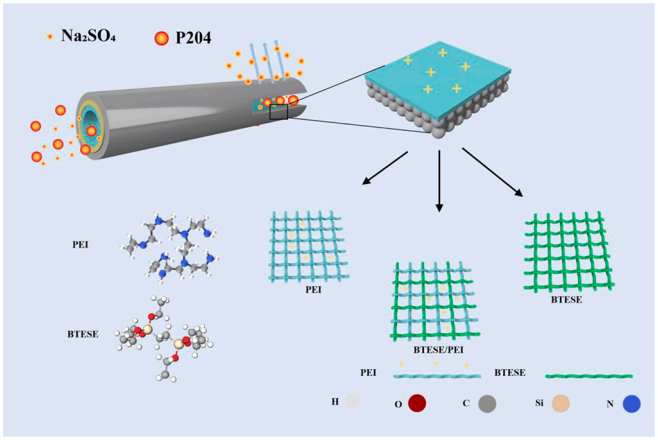


Fig. 11. Schematic diagram of the BTESE-based membranes separation mechanism.

surface exhibits strong electrostatic repulsion toward SO_4^{2-} in the solution. To maintain electroneutrality, Na_2SO_4 is consequently retained on the feed side of the membrane. In contrast, the abundant amino groups in the PEI structure endow the membrane with a strong positive charge, which greatly weakens the barrier effect of the membrane toward Na_2SO_4. As a result, the selective separation of P204 and Na_2SO_4 is achieved through the synergistic effect of pore-size sieving and electrostatic interactions.

3.4. Effect of salt concentration in the P204/Na_2SO_4 system on the separation performance of BP membrane

In practical wastewater treatment applications, effluents containing extractants, such as those containing P204, frequently exhibit elevated concentrations of inorganic salts. A systematic evaluation of the membrane performance under realistic ionic strength conditions was conducted through cross-flow filtration experiments. The experiments utilized the BP-0.1 wt% nanofiltration membrane under constant transmembrane pressure of 5 bar. A series of synthetic feed solutions with Na_2SO_4 concentrations ranging from 1 to 300 mM were prepared, while the P204 concentration was maintained at approximately 100 mg L^{-1}. As illustrated in Fig. 12(a), the rejection (%) of P204 by the BP-0.1 wt% membrane showed a marked decreasing trend with the increasing Na_2SO_4 concentration in the P204/Na_2SO_4 system. When the Na_2SO_4 concentration reached 100 mM, the rejection (%)of P204 sharply decreased to 30.8%. In contrast, the Na_2SO_4 rejection remained relatively unchanged at approximately 17–19% in the Na_2SO_4 concentration range 1–10 mM and only slightly decreased at 100 mM. Overall, at concentrations ranging between 1 and 10 mM of Na_2SO_4, the membrane showed a certain degree of separation performance for P204 and Na_2SO_4. When the Na_2SO_4 concentration further increased to 100 mM, both could permeate the membrane relatively easily, resulting in almost complete loss of separation effect. This result is consistent with the principles of the Donnan exclusion theory, which presents that elevated salt concentration disrupts the electrostatic equilibrium across the membrane. First, increased Na^+ concentration compresses the electrical double layer near the membrane surface. Second, elevated SO_4^{2-} concentrations have been shown to enhance counterion shielding of the positively charged membrane surface. This phenomenon has the potential to induce competitive adsorption and reduce effective surface charge density, which can weaken electrostatic repulsion against cationic or zwitterionic P204 species. Furthermore, the salting-out effect induced by high ionic strength may alter the solvation shell and aggregation behavior of P204, promoting its passage through membrane pores and further diminishing rejection.

Although promising separation performance was observed in controlled laboratory simulations, the pronounced sensitivity of the BP-0.1 wt% membrane to ionic strength raises concerns regarding its robustness in real-world settings. Industrial extraction wastewater contains high concentrations of inorganic salts and complex matrices, including organic degradation by-products, surfactants, and stabilized emulsified droplets. These characteristics collectively impose significantly harsher operational challenges than simplified model systems. To assess engineering viability, the evaluation was therefore extended to actual industrial P204-laden wastewater (Fig. 12(b)), wherein the P204: Na_2SO_4 mass ratio approximated 1:50. Under these conditions, the P204 rejection plummeted to 20.7%, while Na_2SO_4 rejection remained at 14.6%. A clear comparison of these data demonstrates that under actual operating conditions with high salinity and low pollutant concentrations, the selective advantage of the membrane for P204 is no longer evident. This phenomenon is the result of a synergistic effect of two processes: charge shielding, which weakens electrostatic repulsion, and salting-out, which alters the dissolution behavior of P204. Therefore, when treating high-salinity complex systems, the separation performance of the BP-0.1 wt% membrane is significantly constrained, making it unsuitable for meeting the requirements of advanced wastewater

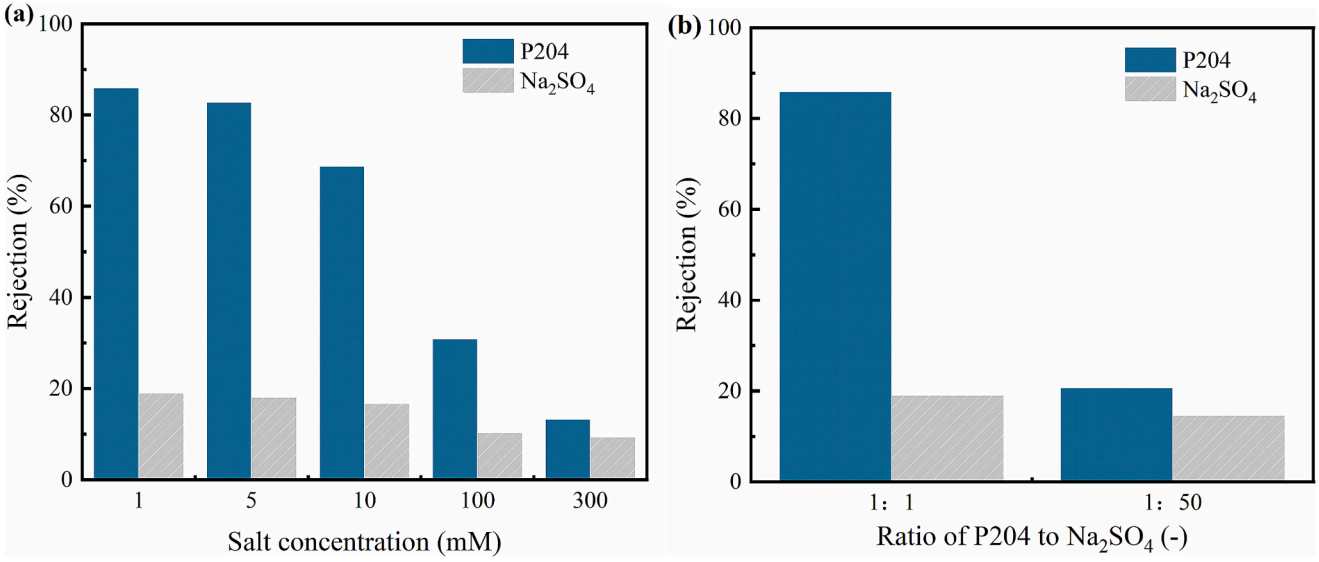


Fig. 12. Rejection of the BP-0.1 wt% membrane for a mixed P204/Na_2SO_4 solution under (a) different salt concentrations and (b) simulated and actual systems.

Table 3
Comparison of removal performance between BTESE/PEI membrane and other materials.

Method	Materials	Feed condition	Evaluation criteria	Water permeance/L m^{-2} h^{-1} bar^{-1}	Rejection/%	Ref.
Resin adsorption	D-201-OH	P507	Adsorption capacity	/	99.2	(Su et al., 2018)
Resin adsorption	DA201-C	P507	Adsorption rate	/	96	(Liu et al., 2022)
Ozone catalytic oxidation	/	P507	TOC	/	95.9	(Wang et al., 2023)
Electrocatalytic oxidation	/	P204/Na_2SO_4	COD	/	93.5	(Wang et al., 2024)
Membrane separation	BP-0.1 wt%	P204/Na_2SO_4	TOC	36.4	85.9	This work

treatment in practical applications.

As shown in Table 3, compared with the currently reported literature, the BP-0.1 wt% membrane described in this study still shows research potential. Through modification and optimization of the membrane material, it is expected to prepare a more advantageous nanofiltration membrane suitable for the separation of such systems. In addition, the stability of the prepared membranes and the PEI-modified layer was not evaluated in the current study. Considering the practical application of separation membranes, the durability and structural stability of the modified layer are crucial. Therefore, exploring the stability of the PEI-modified layer will be one of the main challenges for next stage of this research project.

4. Conclusions

In this study, a positively charged BTESE/PEI composite membrane was fabricated on a tubular Al_2O_3 support via the sol-gel and surface modification for selective separation in the P204/Na_2SO_4 system. The incorporation of PEI enhanced membrane hydrophilicity through hydrogen bonding and increased positive charge density via amino groups, enabling synergistic separation by pore-size sieving and charge interaction.

Under controlled conditions at 5 bar, the optimized BP-0.1 wt% membrane achieved a P204 rejection of 85.9% while reducing Na_2SO_4 rejection to 19.0%, with a pure water permeability of 36.4 L m^{-2} h^{-1} bar^{-1}. In contrast, the unmodified BTESE membrane showed higher rejections for both solutes (P204: 91.0%; Na_2SO_4: 87.7%) and a permeability of 42.3 L m^{-2} h^{-1} bar^{-1}, indicating the effectiveness of PEI in improving selectivity. However, when tested in actual high-salinity wastewater, the separation performance deteriorated significantly: P204 rejection dropped to 20.7%, whereas Na_2SO_4 rejection remained at 14.6%. This decrease is ascribed to the collective impacts of charge shielding, which weakens electrostatic repulsion toward Na_2SO_4 and salting-out, which alters the dissolution behavior of P204. These factors jointly limit the practical applicability of the BP-0.1 wt% membrane in complex saline environments.

Overall, while PEI modification enhances selective separation under ideal conditions, the membrane's performance is considerably constrained in real wastewater systems, highlighting the need for further material optimization toward high-salinity tolerance.

CRediT authorship contribution statement

Yuanyan Liu: Writing – review & editing, Writing – original draft, Visualization. **Xinyu Jiao:** Resources, Formal analysis, Data curation. **Xincheng Pan:** Investigation, Data curation. **Hong Qi:** Supervision, Data curation.

Declaration of competing interest

The authors declare that they have no known competing financial interests or personal relationships that could have appeared to influence the work reported in this paper.

Acknowledgments

This work is supported by the National Natural Science Foundation of China (21490581), China Petroleum & Chemical Corporation (317008-6).

References

Al-Oweini, R., El-Rassy, H., 2009. Synthesis and characterization by FTIR spectroscopy of silica aerogels prepared using several $Si(OR)_4$ and $R''Si(OR')_3$ precursors. J. Mol. Struct. 919 (1–3), 140–145. https://doi.org/10.1016/j.molstruc.2008.08.025.

Bapat, D.U., Dalvi, V.H., 2019. Molecular insights into water clusters formed in tributylphosphate-di-(2-ethylhexyl)phosphoric acid extractant systems from experiments and molecular dynamics simulations. J. Phys. Chem. B 123 (7), 1618–1635. https://doi.org/10.1021/acs.jpcb.8b10831.

Chen, L., Wenjun, S., Zedong, L., Xiuwei, A., Simiao, L., 2020. Ceramic nanocomposite membranes and membrane fouling: a review. Water Res. 175, 115674. https://doi.org/10.1016/j.watres.2020.115674.

Gu, K., Wang, S., Li, Y., Zhao, X., Zhou, Y., Congjie, G., 2019. A facile preparation of positively charged composite nanofiltration membrane with high selectivity and permeability. J. Membr. Sci. 581, 214–223. https://doi.org/10.1016/j.memsci.2019.03.057.

He, Z., Lyu, Z., Gu, Q., Zhang, L., Wang, J., 2019. Ceramic-based membranes for water and wastewater treatment. Colloids Surf. A Physicochem. Eng. Aspects. 578, 123513. https://doi.org/10.1016/j.colsurfa.2019.05.074.

Jiang, X., Dai, B., Zhou, Y., Chang, B., Li, Y., Du, C., Liu, T., 2025. Synthesis of P204 polystyrene resin adsorbents for efficient and selective removal of uranium. J. Radioanal. Nucl. Chem. 334 (2), 1861–1870. https://doi.org/10.1007/s10967-024-09936-2.

Lee, C., Arby, D.S., Kim, C., Lim, J., Kwon, K., Chung, E., 2025. Hydrometallurgical process of spent lithium-ion battery recycling part. 1 chemical leaching of valuable metals from cathode active materials: review and case study. Hydrometallurgy 235, 106494. https://doi.org/10.1016/j.hydromet.2025.106494.

Li, J., Wang, D.K., Tseng, H.-H., Wey, M.-Y., 2021. Solvent effects on diffusion channel construction of organosilica membrane with excellent CO_2 separation properties. J. Membr. Sci. 618, 118758. https://doi.org/10.1016/j.memsci.2020.118758.

Li, Y., Gao, Y., Zhu, Y., Zhang, H., Zhang, W., Yin, Y., Zhang, Y., Wang, C., 2024. Fabrication of self-cleaning nanofiltration membranes through interfacial polymerization using PEI@CoPc monomer for Mg^{2+}/Li^{+} separation. Chem. Eng. J. 496, 153807. https://doi.org/10.1016/j.cej.2024.153807.

Lim, J., Jang, Y., Lee, J., Lee, C., Jbari, O., Kwon, K., Chung, E., 2025. Hydrometallurgical process of spent lithium-ion battery recycling part. 2 recovery of valuable metals from the cathode active material leachates: review and cost analysis. Hydrometallurgy 236, 106516. https://doi.org/10.1016/j.hydromet.2025.106516.

Lin, C., Fang, L., Du, S., Yao, Z., Zhu, B., 2019. A novel positively charged nanofiltration membrane formed via simultaneous cross-linking/quaternization of poly(m-phenylene isophthalamide)/polyethyleneimine blend membrane. Sep. Purif. Technol. 212, 101–109. https://doi.org/10.1016/j.seppur.2018.11.026.

Liu, T., Chen, J., Li, H., Li, K., Li, D., 2019. Further improvement for separation of heavy rare earths by mixtures of acidic organophosphorus extractants. Hydrometallurgy 188, 73–80. https://doi.org/10.1016/j.hydromet.2019.06.008.

Liu, D., Zhang, Y., Zheng, X., Qi, S., Zhao, L., Feng, Z., 2022. Adsorption and recovery of P507 extractant from rare earth raffinate by macroporous adsorption resin. J. Chin. Soc. Rare Earths. 40 (06), 1090–1097. https://doi.org/10.11785/S1000-4343.20220617.

Luan, W., Nie, C., Chen, X., Tang, Z., Qiu, M., Fan, Y., 2022. Effective construction of anti-fouling zwitterion-functionalized ceramic membranes for separation of oil-in-water emulsion based on PDA/PEI co-deposition. J. Environ. Chem. Eng. 10 (5), 108396. https://doi.org/10.1016/j.jece.2022.108396.

Luo, J., Li, J., Lin, L., 2015. Solvent extraction of calcium ion from cation-exchange resin regeneration wastewater using D2EHPA and saponified D2EHPA. Desalin. Water Treat. 53 (5), 1286–1291. https://doi.org/10.1080/19443994.2013.852134.

Nakahiro, K., Yu, L., Nagasawa, H., Tsuru, T., Kanezashi, M., 2021. Pore structure controllability and CO_2 permeation properties of silica-derived membranes with a dual-network structure. Ind. Eng. Chem. Res. 60 (23), 8527–8537. https://doi.org/10.1021/acs.iecr.1c00872.

Ngamou, P.H.T., Overbeek, J.P., Kreiter, R., van Veen, H.M., Vente, J.F., Wienk, I.M., Cuperus, P.F., Creatore, M., 2013. Plasma-deposited hybrid silica membranes with a controlled retention of organic bridges. J. Mater. Chem. A 1 (18), 5567–5576. https://doi.org/10.1039/c3ta00120b.

Nicolini, J.V., Borges, C.P., Ferraz, H.C., 2016. Selective rejection of ions and correlation with surface properties of nanofiltration membranes. Sep. Purif. Technol. 171, 238–247. https://doi.org/10.1016/j.seppur.2016.07.042.

Oh, K.H., Ko, Y.-H., Kim, K.-J., 2020. Mechanical properties of amorphous PEI, PES, and PVC up to 11 GPa studied by Brillouin light scattering. Physica B Condens. Matter. 576, 411722. https://doi.org/10.1016/j.physb.2019.411722.

Su, W., Chen, J., Deng, Y., Yang, M., Liu, C., 2018. Recovery of organphosphorus extractants from water by anion exchange resin. Chin. J. Appl. Chem. 35 (07), 802–811. https://doi.org/10.11944/j.issn.1000-0518.2018.07.170321.

Suhalim, N.S., Kasim, N., Mahmoudi, E., Shamsudin, I.J., Mohammad, A.W., Mohamed Zuki, F., Jamari, N.L.-A., 2022. Rejection mechanism of ionic solute removal by nanofiltration membranes: an overview. Nanomaterials 12 (3), 437. https://doi.org/10.3390/nano12030437.

Wai Lin, S., Perez Sicairos, S., Felix Navarro, R.M., 2007. Preparation, characterization and salt rejection of negatively charged polyamide nanofiltration membranes. J. Mex. Chem. Soc. 51 (3), 129–135.

Wang, W., Shi, J., Luo, J., Ma, D., Huang, X., Zhou, Y., 2023. Efficient treatment of P507 wastewater from ternary lithium battery industry by ozone catalytic oxidation technology. Mod. Chem. Ind. 43 (S2), 214–218. +224. 10.16606/j.cnki.issn0253-4320.2023.S2.042.

Wang, C., Li, L., Song, L., Zhang, Y., Liu, S., He, C., 2024. Experimental study on treatment of P204-containing wastewater by threedimensional electrocatalytic oxidation. Ind. Water Wastewater. 55 (04), 31–36.

Wu, X., Liu, H., Qi, H., 2020. Fabrication of tubular organic-inorganic hybrid SiO_2 nanofiltration membrane derived from silsesquioxane. J. Nanjing Tech Univ. (Nat. Sci. Ed.). 42 (01), 94–100. https://doi.org/10.3969/j.issn.1671-7627.2020.01.014.

Xiang, P., Liu, Y.X., Qin, N., Zhang, Y.Y., Xu, L.N., Huang, X., Gao, D.L., Chen, J.H., Yang, Q., 2025. Preparation of PEI/COFs-NH_2PES composite nanofiltration membranes via polyelectrolyte polyethyleneimine-mediated assembly and their study on dye/salt separation. J. Membr. Sci. 718, 123652. https://doi.org/10.1016/j.memsci.2024.123652.

Xing, C., Liu, C., Lai, C., Zhang, S., 2023. Tuning d-spacing of graphene oxide nanofiltration membrane for effective dye/salt separation. Rare Metals 42 (2), 418–429. https://doi.org/10.1007/s12598-022-02153-4.

Xu, R., Liu, Q., Ren, X., Lin, P., Zhong, J., 2020. Tuning the pore satructures of organosilica membranes for enhanced desalination performance via the control of calcination temperatures. Membranes 10 (12), 392. https://doi.org/10.3390/membranes10120392.

Yang, Y., Walton, A., Sheridan, R., Güth, K., Gauß, R., Gutfleisch, O., Buchert, M., Steenari, B.-M., Van Gerven, T., Jones, P.T., Binnemans, K., 2016. REE recovery from end-of-life NdFeB permanent magnet scrap: a critical review. J. Sustainable Metall. 3 (1), 122–149. https://doi.org/10.1007/s40831-016-0090-4.

Zhan, W., Zhen, A., Yu, X., Zhang, J., Li, B., Chen, J., Zhao, H., Chen, H., 2020. Recovery Method for Valuable Metals in Waste Nickel-Cobalt-Manganese Ternary Lithium Batteries. WO 2020/220559 A1, PCT Patent, Publication 05 November 2020. https://patentscope.wipo.int/search/en/detail.jsf?docId=WO2020220559.

Zhang, H., He, D., Niu, S., Qi, H., 2021. Tuning the microstructure of organosilica membranes with improved gas permselectivity via the co-polymerization of 1,2-bis(triethoxysilyl) ethane and 1,2-bis(triethoxysilyl)methane. Int. J. Hydrog. Energy 46 (33), 17221–17230. https://doi.org/10.1016/j.ijhydene.2021.02.139.

Zhang, A., Guan, K., Mai, Z., Wang, Z., Dai, L., Li, C., Li, B., Li, Z., Hu, M., Zhang, P., Matsuyama, H., 2025. Polar pore surface of polyamide membranes enabling efficient solvent mixture separation. Adv. Funct. Mater. 35 (23), 2422376. https://doi.org/10.1002/adfm.202422376.

Zheng, F.-T., Qu, J., Sun, Z., 2022. Preparation of nanocomposite aromatic polyamide reverse osmosis membranes by in-situ polymerization of bis(triethoxysilyl)ethane (BTESE). J. Membr. Sci. 661, 120914. https://doi.org/10.1016/j.memsci.2022.120914.